

SLIP-TYPE BOUNDARY CONDITIONS FOR TURBULENT FLOWS OVER HETEROGENEOUS ROUGHNESS

Jonathan Neuhauser, Kay Schäfer, Davide Gatti, Bettina Frohnäpfel

Institute of Fluid Mechanics

Karlsruhe Institute of Technology (KIT)

Kaiserstraße 12, 76131 Karlsruhe, Germany

jonathan.neuhauser / kay.schaefer / davide.gatti / bettina.frohnäpfel@kit.edu

ABSTRACT

Turbulent flow over a surface with laterally varying roughness is studied by means of direct numerical simulations (DNS) in a channel. It is known that this configuration gives rise to secondary flows which affect the mean momentum and heat transport. We prescribe spanwise varying wall properties by means of anisotropic slip, which allows to study both ridge- and strip-type roughness without the need for a geometrical representation of the surface structure.

INTRODUCTION

Secondary flows of Prandtl’s second kind, i.e. nonzero mean values of the transverse velocity components are known to occur in wall-bounded flows with spanwise inhomogeneous roughness distribution (strip-type roughness, Hinze (1967)) and streamwise aligned ridges (Vanderwel & Ganapathisubramani, 2015). Their strength amounts to a few percent of the mean flow velocity only. Despite this relatively weak intensity, they can strongly alter the mean flow field, and, in consequence, the drag and heat transfer properties of a turbulent boundary layer (see e.g. Stroh *et al.* (2020a)).

While the numerical resolution of surface roughness can be achieved, it often induces stricter mesh requirements than for smooth wall simulations. Therefore, roughness models to be used within flow-scale resolving simulations can enable the investigation of roughness effects at higher Reynolds numbers and in complex flow scenarios. In the present study we employ a slip length boundary condition to prescribe spanwise inhomogeneous roughness. Such a boundary condition has been used as a model for textured surfaces such as drag-reducing riblets (Luchini *et al.*, 1991), superhydrophobic surfaces (Min & Kim, 2004) and general rough surfaces (Luchini, 2013). This boundary condition is chosen because a nonzero slip length for the spanwise velocity component enhances near-wall turbulence (Min & Kim, 2004), while at the same time leaving laminar flow unaffected. The present contribution aims to investigate the suitability of a boundary condition based on spanwise slip for modelling spanwise heterogeneous roughness. In addition, we investigate to which extent a streamwise slip length may be used to account for spanwise elevation differences.

METHODOLOGY

We solve the Navier-Stokes equations for the incompressible flow of a Newtonian fluid subject to spanwise heterogeneous slip-length boundary conditions (Navier, 1823)

$$u_{y=0} = l_{s,u}(z) \frac{\partial u}{\partial y} \Big|_{y=0}, \quad w_{y=0} = l_{s,w}(z) \frac{\partial w}{\partial y} \Big|_{y=0} \quad (1)$$

Table 1: Grid properties. The box size $L_x \times L_y \times L_z$ is $8\delta \times 2\delta \times 4\delta$, except for cases with $b/\delta = 4$ ($L_z = 16\delta$).

Re_τ	$N_x \times N_y \times N_z$	Δz^+	Δy_{\min}^+	Δz^+
180	$256 \times 193 \times 128$	5.625	1.001	5.625
540	$768 \times 451 \times 384$	5.625	1.003	5.625

by means of direct numerical simulation (DNS). Streamwise, wall-normal and spanwise directions are denoted through x , y and z , respectively; the corresponding instantaneous velocity components are u , v and w . The problem considered is a doubly-periodic channel as sketched in Fig. 1 subject to constant pressure gradient (CPG) forcing. The boundary conditions employed at top and bottom wall are symmetric around the channel centerline with a spanwise strip width s .

In order to characterize the correspondence of $l_{s,w}$ to traditional roughness measures, homogeneous reference cases are considered. The DNS in this work are performed using the solver XCompact3D (Bartholomew *et al.*, 2020) at $Re_\tau = 180$ and $Re_\tau = 540$ (homogeneous reference only). In the streamwise and spanwise directions, the mesh is homogeneous; in the wall normal direction stretching is used to refine the mesh towards the wall such that the first node is placed at $y^+ = 1$. The mesh properties are given in Table 1. All turbulent properties denoted with $\langle \cdot \rangle$ correspond to averages that exploit all symmetries of the set-up, including phase averaging. Additionally, $\bar{\cdot}$ denotes quantities that are averaged in such a way that they are independent of the spanwise coordinate z , i.e. $\bar{u}(y) = \frac{1}{2s} \int_0^{2s} \langle u \rangle(y, z) dz$. The superscript $+$ indicates nondimensionalization in wall units.

RESULTS

Spanwise slip

Slip lengths are a well-researched model for textured surfaces, mostly in form of protrusion heights (Luchini *et al.*, 1991). It has been established that a transversal slip increases near-wall turbulence and thus skin-friction drag; while a longitudinal slip shifts the mean velocity profile (increasing the flow rate under CPG) (Min & Kim, 2004). A combination of spanwise and streamwise slip may serve as a virtual wall (Gómez-de-Segura & García-Mayoral, 2020). In order to relate the dimensionless spanwise slip length to well-known properties of homogeneously rough surfaces, a series of DNS simulations at $Re_\tau = 180$ and $Re_\tau = 540$ were carried out, the results of which are displayed in Fig. 2. The relative velocity deficit

$\Delta U^+ = \langle u \rangle^+|_{\delta} - \langle u \rangle^+|_{\delta, \text{NSBC}}$ monotonously increases with the slip length and collapses well for both Reynolds numbers.¹

The strip-type configuration is investigated in a parameter study for different patch sizes $s/\delta = 0.25..16$ at $Re_{\tau} = 180$ with a spanwise slip length of $l_{s,w} = 0.05\delta$ ($l_{s,w}^+ = 9$). The results reveal – for all strip size ratios – a pair of secondary vortices that yields upwelling in the no-slip (smooth) region and downwelling in the spanwise-slip (rough) region, independent of the strip width. The vortices are of approximately square size, i.e. confined to a region near the wall in case of narrow strips (see Fig. 3(a)), and space-filling only for $s \approx \delta$ (Fig. 3(c)). The momentum distribution is strongly dependent on the strip width and shows different behavior in the limiting cases of small and large strips. For narrow strips ($s = 0.25\delta$), the influence of the inhomogeneity is limited to a region near the wall; the outer layer is nearly homogeneous.

For $s \gg \delta$, the flow prefers the path of least resistance (i.e. the no-slip region) and consequently a high momentum pathway is located over this region (see Fig. 3(b)). For $s \approx \delta$, the secondary flow has the strongest impact on the momentum distribution in the channel. The secondary motion induces an upwelling above the no-slip region, thus generating a low momentum pathway in this region. The location of high- and low-momentum pathways is therefore opposite for $s \approx \delta$ and $s \gg \delta$. These results are consistent with the boundary layer experiments by Wangsawijaya *et al.* (2020) and also partly in agreement with DNS results based on the prescription of wall shear stress (Chung *et al.*, 2018).

In contrast to those existing DNS studies the present configuration allows a direct evaluation of the skin friction coefficient which is significantly increased through the presence of the secondary flow for $s \gtrsim \delta$. The global skin friction coefficient is not only governed by the relationship between C_f and $l_{s,w}$, but also by additional contributions from the secondary flow. In order to quantify the latter, we assume that the skin friction coefficient in flows with roughness strips but without any secondary motion can be computed based on the limiting case of two non-interacting channel parts (one smooth and one rough) that are both driven by the same pressure gradient (same $\bar{u}\bar{\tau}$). The identical pressure gradient in both channel part ensures that no spanwise pressure gradient is generated which in turn could drive a spanwise mean flow. The resulting flow rate for these two channel parts will naturally differ and the mean flow rate between the channels is given by $U_b = \frac{1}{2}(U_{b,\text{rough}} + U_{b,\text{smooth}})$. The definition of the skin friction coefficient $C_f = 2\bar{u}\bar{\tau}^2/U_b^2$ then yields an expected global skin friction coefficient of

$$C_f = \left(\frac{1}{2} \left(\frac{1}{\sqrt{C_{f,\text{rough}}}} + \frac{1}{\sqrt{C_{f,\text{smooth}}}} \right) \right)^{-2}, \quad (2)$$

The obtained value in comparison with the computed C_f for different s/δ is displayed in Fig. 4 in which C_f of the smooth and rough homogeneous reference cases is also included. which is the ($p = -\frac{1}{2}$) power mean of the local skin friction coefficients. For the limiting case of small patches, eqn. (2) correctly predicts the global skin friction coefficient. For patch sizes $s/\delta \approx 1$, the pronounced secondary flow is expected to increase the global skin friction coefficient, which is indeed the case. For very large patches $s/\delta \gg 1$, the secondary

flow occupies only a small part of the channel (at the interface between the patches) and has thus little influence on C_f , so (2) holds again. Further elaboration on the interpretation of the skin friction coefficient in a spanwise inhomogeneous setting is given in Neuhauser *et al.* (2022).

The results of the cases with spanwise slip are compared with strip-type roughness IBM data presented in Schäfer *et al.* (2022). Their DNS simulation featured IBM-resolved roughness strips, while the elevation of the smooth strip was changed to investigate the influence of the roughness protrusion. A direct comparison between the results is shown in Fig. 5. The mean velocity profile, Reynolds stress and secondary flow agree well, in particular with the IBM case of slightly recessed roughness. (The IBM-resolved roughness has a mean (meltdown) height of $\bar{k}/\delta = 0.043$, with tips protruding to $k_{\text{max}}/\delta = 0.1$; the smooth surface is located at $y = 0.07525\delta$). Shown alongside the IBM and SLBC results are the results of a parametric forcing (PFA) model from Schäfer *et al.* (2022). In general, the turbulence properties of the SLBC case show good qualitative agreement with the ones found over slightly recessed roughness strips (for PFA: $h = 2.5\bar{k}$, displayed in Fig. 5(c), (f), (i)). The gray area represents the PFA modelled roughness area and the white area the elevated smooth wall. Note that the friction Reynolds number is higher for PFA and IBM data ($Re_{\tau} = 500$) than for the present cases. While the more complex PFA model is able to capture the effects at the corners of the roughness, the bulk of the flow is well captured with the SLBC model as well.

The question immediately arises whether it's possible to model different roughness heights or, by extension, strip-type roughness (at least for small elevations) in a slip length framework as well. In this context, we investigate the combination of spanwise and streamwise slip.

Spanwise and streamwise slip

Based on a virtual origin framework (Gómez-de-Segura & García-Mayoral, 2020), a combination of slip lengths for the three velocity components may be used to impose a wall (rough or smooth) at a given elevation, as long as the elevation is small compared to the channel height. The spanwise slip (also wall-normal slip, but this is not considered here) sets the origin of turbulence, while the streamwise slip sets the origin of the mean flow. These virtual origins are the (typically negative) wall-normal lengths by which the mean profile or the Reynolds stresses would have to be shifted in order to collapsed with those of a canonical channel. If the origin of turbulence l_T^+ and the origin of the mean flow l_U^+ both are equal and positive, this corresponds to a recessed wall. (Increasing l_T^+ further represents a rough recessed wall.) This can be used to model ridge-type roughness, assuming that the height of the ridges is below $h^+ \lesssim 10$, because otherwise the near-wall turbulence cycle would be clipped by the simulation box. As discussed in Gómez-de-Segura & García-Mayoral (2020), the spanwise slip length $l_{s,w}^+$ and l_T^+ are not identical, the underlying saturation effect is also discussed in Fukagata *et al.* (2006) and displayed in Fig. 2. For $l_{s,u}^+ = 9$ and $l_{s,w}^+ = 13.5$, such a recessed wall is achieved. Indeed, such a combined boundary condition is able to reverse the direction of the secondary flow, see Fig. 3(e). This matches IBM data from von Deyn *et al.* (2021) for ridges of relatively small height; in the configuration of Fig. 3(e), the ridge corresponds to the no-slip part of the wall. It also bears resemblance to slightly protruding roughness strips as seen in Stroh *et al.* (2020b) and Schäfer *et al.* (2022), suggesting that the flow topology in such a case is dominated by the protrusion and not by the roughness. In

¹Due to the relatively low Reynolds number, the difference of mean centerline velocity is used for the computation of ΔU^+ instead of evaluating the logarithmic law.

this case, no pronounced high- or low momentum pathways can be recognized.

It is apparent that the case of a recessed wall (3(e)) can be constructed as the superposition of the cases with only one component of slip, i.e. $l_{s,w}^+ = 13.5$ (Fig. 3(c) displays $l_{s,w}^+ = 9$) and $l_{s,u}^+ = 9$ (displayed in Fig. 3(d)). While it is difficult to interpret the boundary condition for Fig. 3(d) as a physical wall; in particular, there are no deflections of spanwise fluctuations, since the boundary condition for w is identical over both strips. The results are still relevant as part of a decomposition of ridge-type roughness. The part of the channel with elevated streamwise slip (ESS) naturally has higher streamwise velocity $\langle u \rangle$ at $y = 0$, but the velocity at the centerline is higher over the no-slip region. The orientation of the streamwise secondary vortices is consistent with this observation, i.e. downwelling (upwelling) in the z region of the high (low) momentum pathway, respectively. The ESS strips increase the overall flow rate of the channel, reducing the skin friction coefficient. The flow response to the combined boundary condition (Fig. 3(e)) also appears to be well-captured by a superposition of the cases Fig. 3(c) and Fig. 3(d), which feature slip only in one direction, respectively. The streamwise velocity and skin friction coefficient behaves as the average of the two cases, while the secondary flow resembles the sum of the respective secondary flow patterns.

By switching the relative position of the regions of elevated u and w slip, the secondary flow can be strongly enhanced; both effects – due to roughness and ESS – induce identically oriented streamwise rolls. This is shown in Fig. 3(f). Such an increase in secondary flow magnitude should correspond to an increase in skin friction, and indeed, the skin friction coefficient is approx. 25% higher in case of Fig. 3(f) than in Fig. 3(e), even after correcting for the lower w slip length.

Generally, the skin friction coefficient in absence of secondary flow can be computed with Eq. (2). The decrease of skin friction in areas of streamwise slip must be taken into account, which avoids establishing an effective channel height. The decomposition of the skin friction coefficient in this case will be further analyzed at the conference.

Note that Fig. 3(f) is not equal to a rough ridge; this would require $l_T^+ = l_U^+$ in the region of streamwise slip.

CONCLUSION AND OUTLOOK

The current study demonstrates the possibility to model spanwise inhomogeneous roughness based on spanwise and streamwise slip. The boundary condition correctly predicts the orientation and size of the secondary flow and the location of low and high momentum pathways for strip-type roughness (spanwise slip only) and roughness consisting of shallow ridges (combination of spanwise and spanwise slip). One important property of the proposed model for strip-type roughness is the fact that it does not alter laminar flow behavior. It thus enables to study the impact of heterogeneous surface roughness onto turbulence without artefacts that are generated when the laminar flow behavior is modified through the boundary conditions as it is e.g. the case with the prescription of laterally varying shear stress. Additionally, the estimation of the skin friction coefficient C_f is discussed. Further comparisons between data for elevated/recessed roughness strips, (shallow) ridge type roughness and the corresponding slip length models will be shown at the conference. Slip lengths thus provide a very simplified, but unified framework to study different canonical roughness configuration in DNS.

ACKNOWLEDGEMENTS

We gratefully acknowledge the financial support of DFG through project 237267381-TRR150 and support by the state of Baden-Württemberg through bwHPC.

REFERENCES

- Bartholomew, P., Deskos, G., Frantz, R. A. S., Schuch, F. N., Lamballais, E. & Laizet, S. 2020 Xcompact3d: An open-source framework for solving turbulence problems on a cartesian mesh **12**, 100550.
- Chung, D., Monty, J. P. & Hutchins, N. 2018 Similarity and structure of wall turbulence with lateral wall shear stress variations. *Journal of Fluid Mechanics* **847**, 591–613.
- von Deyn, L. H., Gatti, D., Frohnappfel, B. & Stroh, A. 2021 Parametric study on ridges inducing secondary motions in turbulent channel flow. *Proc. Appl. Math. Mech.* **20** (1), e202000139.
- Fukagata, Koji, Kasagi, Nobuhide & Koumoutsakos, Petros 2006 A theoretical prediction of friction drag reduction in turbulent flow by superhydrophobic surfaces. *Physics of Fluids* **18** (5), 051703.
- Gómez-de-Segura, G. & García-Mayoral, R. 2020 Imposing virtual origins on the velocity components in direct numerical simulations. *International Journal of Heat and Fluid Flow* **86**, 108675.
- Hinze, J. O. 1967 Secondary currents in wall turbulence. *Phys. Fluids* **10** (9), S122.
- Luchini, P. 2013 Linearized no-slip boundary conditions at a rough surface. *Journal of Fluid Mechanics* **737**, 349–367.
- Luchini, P., Manzo, F. & Pozzi, A. 1991 Resistance of a grooved surface to parallel flow and cross-flow. *Journal of Fluid Mechanics* **228**, 87.
- Min, T. & Kim, J. 2004 Effects of hydrophobic surface on skin-friction drag. *Physics of Fluids* **16** (7), L55–L58.
- Navier, C. L. M. H. 1823 Mémoire sur les lois du mouvement des fluides. *Mémoires de l'Académie Royale des Sciences de l'Institut de France* **6** (1823), 389–440.
- Neuhauser, J., Schäfer, K., Gatti, D. & Frohnappfel, B. 2022 Simulation of turbulent flow over roughness strips. *submitted to Journal of Fluid Mechanics*.
- Schäfer, K., Stroh, A., Forooghi, P. & Frohnappfel, B. 2022 Modelling spanwise heterogeneous roughness through a parametric forcing approach. *Journal of Fluid Mechanics* **930**.
- Stroh, A., Schäfer, K., Forooghi, P. & Frohnappfel, B. 2020a Secondary flow and heat transfer in turbulent flow over streamwise ridges. *International Journal of Heat and Fluid Flow* **81**, 108518.
- Stroh, A., Schäfer, K., Frohnappfel, B. & Forooghi, P. 2020b Rearrangement of secondary flow over spanwise heterogeneous roughness. *J. Fluid Mech.* **885**.
- Vanderwel, C. & Ganapathisubramani, B. 2015 Effects of spanwise spacing on large-scale secondary flows in rough-wall turbulent boundary layers. *Journal of Fluid Mechanics* **774**.
- Wangawijaya, D. D., Baidya, R., Chung, D., Marusic, I. & Hutchins, N. 2020 The effect of spanwise wavelength of surface heterogeneity on turbulent secondary flows. *J. Fluid Mech.* **894**.

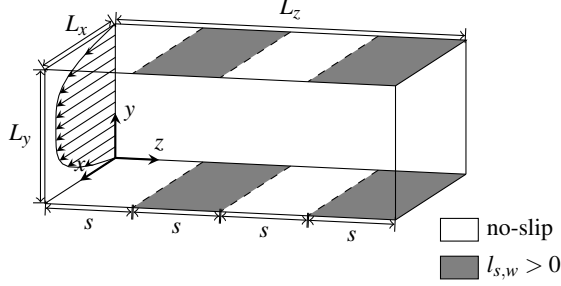


Figure 1: A sketch of the channel with spanwise variable slip length. The configuration shown here corresponds to strip-type roughness (Fig. 3(c)).

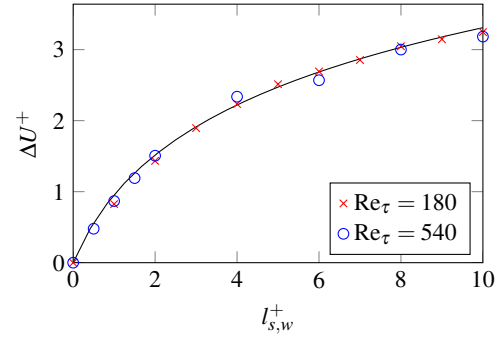


Figure 2: Relative velocity deficit $\Delta U^+ = \langle u \rangle^+|_{\delta} - \langle u \rangle^+|_{\delta, \text{NSBC}}$ for $\text{Re}_\tau = 180$ and $\text{Re}_\tau = 540$ and (solid line) Logarithmic approximation $1.38 \ln(l_{s,w} + 1)$.

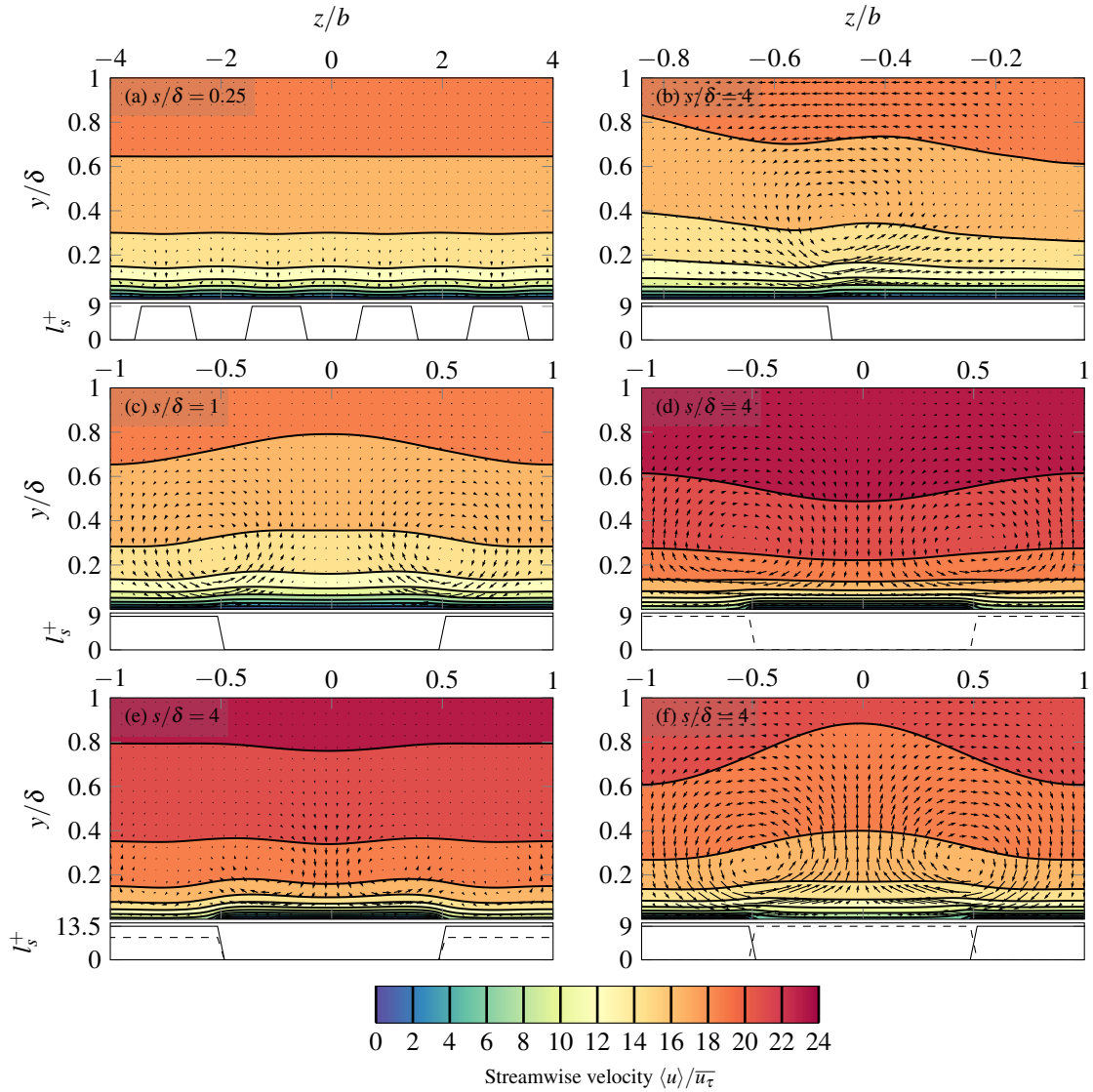


Figure 3: Momentum distribution and secondary flow for different cases of piecewise constant slip length. Contours: time averaged streamwise velocity in the yz plane. The secondary flow $[\langle v \rangle, \langle w \rangle]/u_\tau$ in the plane is indicated with vectors, with equally scaled length among the plots. Below the plots the respective boundary configuration is given; solid line: $l_{s,w}$, dashed line: $l_{s,u}$. (a), (b), (c): Different spanwise wavelengths of $l_{s,w}$; the first two show the limiting behavior, the third an intermediate case. (d): u -slip only. (e) and (f) are combined cases; (e) represents recessed ridges based on a virtual origin approach ($l_T \approx l_U$), (f) increases the strength of the secondary flow by constructive interference of the flow topology for streamwise and spanwise slip only.

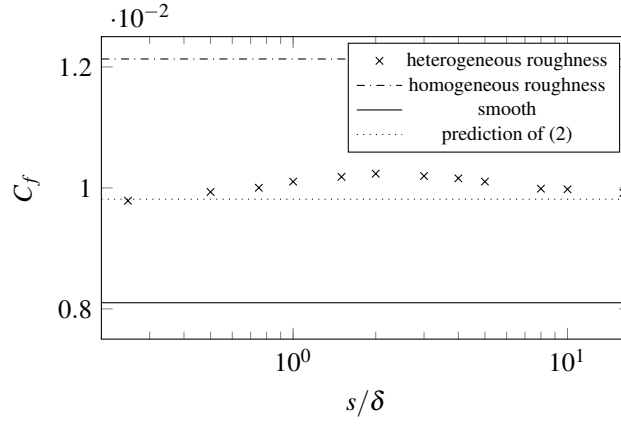


Figure 4: Skin friction coefficient C_f as a function of the strip width s/δ with step-wise change of the boundary condition and $l_{s,w,max}^+ = 9$ in the rough patch. C_f for the standard smooth wall, the homogeneous rough case with $l_{s,w}^+ = 9$ and the prediction based on Eqn. (2) are included for reference.

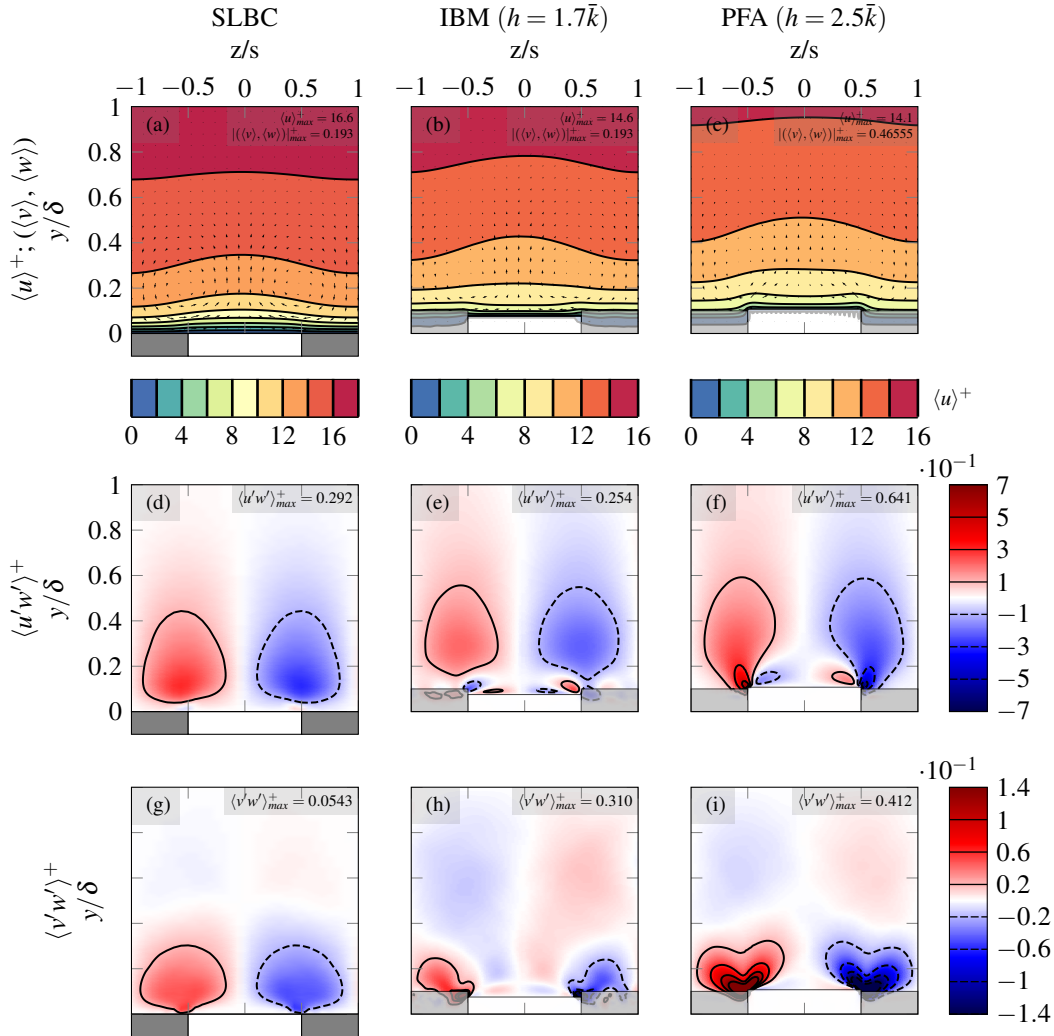


Figure 5: Comparison of SLBC ($l_{s,w,max}^+ = 9, l_{s,u}^+ = 0$ with reference data in form of IBM-resolved roughness from Schäfer *et al.* (2022). All cases at $s/\delta = 0.5$; the simulations are arranged in columns. $s/\delta = 0.5$. First row: Mean streamwise velocity $\langle u \rangle^+$ resp. $(\langle u \rangle - \bar{u}(y=0))^+$ for SSBC), secondary flow (vectors, same scaling in viscous units), second row: $\langle u'w' \rangle^+$, third row: $\langle v'w' \rangle^+$.